biophysica

MDPI

Article

Enhanced Adsorption of Cage-Shaped Proteins on Carbon Surfaces by Carbon Nanotube (CNT)-Binding Peptide Aptamers

Narangerel Ganbaatar [1], Ting-Chieh Chu [1], Naofumi Okamoto [2], Kenji Iwahori [1], Masakazu Nakamura [2] and Ichiro Yamashita [1,*]

[1] Graduate School of Engineering, Osaka University, 2-8 Yamadaoka, Suita 565-0871, Osaka, Japan
[2] Division of Materials Science, Nara Institute of Science and Technology, Ikoma 630-0192, Nara, Japan; mnakamura@ms.naist.jp (M.N.)
* Correspondence: yamashita@jrl.eng.osaka-u.ac.jp

Abstract: The adsorption behavior of recombinant cage-shaped proteins with carbon nanotube (CNT)-binding peptides on carbon surfaces was quantitatively and dynamically analyzed using a highly stable quartz crystal microbalance (QCM). Two types of CNT-binding peptide aptamers obtained by the phage display method were attached to the N- and C-termini of the Dps (DNA-binding protein derived from starved cells) to produce carbonaceous material-binding Dps. The carbon adsorption ability of the mutant Dps was studied by QCM measurement using a carbon-coated QCM sensor. The produced peptide aptamer-modified Dps showed higher affinity than a wild Dps and also showed higher adsorption capacity than a previously used Dps with carbon nanohorn-binding peptides. The newly obtained peptide aptamers were proven to provide Dps with high adsorption affinity on carbon surfaces. Furthermore, the aptamer modified to the N-terminus of the Dps subunit showed more efficient adsorption than the aptamers attached to the C-terminus of the Dp, and the linker was found to improve the adsorption ability.

Keywords: QCM; Dps; aptamer; phage display; CNT

Citation: Ganbaatar, N.; Chu, T.-C.; Okamoto, N.; Iwahori, K.; Nakamura, M.; Yamashita, I. Enhanced Adsorption of Cage-Shaped Proteins on Carbon Surfaces by Carbon Nanotube (CNT)-Binding Peptide Aptamers. *Biophysica* **2024**, *4*, 256–266. https://doi.org/10.3390/biophysica4020018

Academic Editor: Danilo Milardi

Received: 15 April 2024
Revised: 13 May 2024
Accepted: 22 May 2024
Published: 24 May 2024

1. Introduction

For the application of proteins in nanodevice engineering, it is essential to study selective protein adsorption on various solid surfaces. Proteins are amphiphilic and inherently surface-active molecules. Many studies have previously found that different surface chemistries and charges had significant influences on the interaction between protein and inorganic materials involving electrostatic, hydrophobic, hydrogen bonding, and van der Waals interactions. The determination of the dominant interaction and its effect on the protein absorbability is a challenging issue due to many inter-related mechanisms and the complexity of the liquid/solid system. However, measuring and understanding the adsorption behavior of proteins on solid surfaces is an essential and indispensable area of study in many research fields. The study of adsorption is a critical first step in nanofabrication technologies [1–3], biosensors [4], food processing [5], clinical diagnostics [6], drug delivery, disease detection, and biomedical implants [7–9]. Ferritin-family proteins, which are cage-shaped proteins, are protein supramolecules widely spread in nature from bacteria and animals to plants and have attracted much attention due to their application in nanodevice fabrication [10–20]. Ferritin and *Listeria innocua* Dps (DNA-binding protein from starved cells) have been used as chemical reaction vessels, and several kinds of nanoparticles have been synthesized and selectively placed at targeted positions on substrates to fabricate nanostructures for nanoelectronic devices. The key to the nanostructured placement of proteins with nanoparticle cores at designated device locations is to control the selective adsorption of proteins by peptide aptamers genetically immobilized on the outer surface. Therefore, studies have been conducted on the adsorption of peptide aptamers on inorganic

materials such as metallic materials [20–22], inorganic compounds such as silicon dioxide (SiO_2) [23], and carbon nanomaterials [24,25]. By controlling adsorption, the proteins work as self-assembled nano-building blocks, combining with semiconductor processes to create new composite structures with high magnetoconductivity, electro-optical properties, and physicochemical properties [7,16–18].

Recently, we produced a new thermoelectric material, a carbon nanotube (CNT) network with heterojunctions, CNT/Dps (inside core)/CNT [1]. Dps has an outer diameter of 9.5 nm and an inner diameter of 4.5 nm and consists of 12 subunits [26]. A compound semiconductor nanoparticle was synthesized inside. Carbon nanohorn-binding peptides were immobilized on the outer surface of the protein shell, carbon nanohorn-binding Dps (CNHB-Dps). The aptamer worked to form heterojunctions. The fabricated CNT network exhibited low thermal conductivity and high electron mobility due to the heterojunction. Phonons were blocked at the heterojunction due to the difference in mechanical stiffness between the CNTs and the protein shell, while electrons went through the heterojunction by the tunneling effect using nanoparticles in the Dps. In the fabrication of this heterojunction structure, adsorption between Dps and CNT by the peptide aptamers was critically important. However, there was a lack of binding strength between CNTs and carbon nanohorn-binding peptides. Peptide aptamers with higher adsorption strengths need to be obtained, and the obtained aptamers need to be immobilized on the outer surface to produce Dps with higher adsorption capacity than CNHB-Dps.

We have recently obtained CNT-binding peptide aptamers consisting of 12 amino acids using a phage display method [25]. The obtained peptide aptamers showed significantly higher adsorption capacity on carbon surfaces compared to ordinary peptides. If they were immobilized on the outer surface of Dps, a stronger adsorption capacity on carbon surfaces than CNHB-Dps could be expected. However, there were several options for immobilization on Dps, and it was anticipated that the adsorption capacity would vary depending on the method of immobilization. In this study, two of the obtained aptamers with particularly high binding capacities were immobilized on the outer surface of Dps. The immobilization was performed by genetically adding them to the N- or C-terminus of the Dps subunit, or through a linker. We quantitatively measured and analyzed their adsorption behavior on the carbon surface using a quartz crystal microbalance (QCM). The QCM technique, widely acknowledged for its efficacy in examining peptide adsorption on varied substrates like SiO_2 and polystyrene, has been previously employed in similar investigations [27,28]. Our quantitative analysis revealed that the newly obtained Dps exhibited enhanced adsorption capabilities on carbon surfaces. They adsorbed more on carbon surfaces than wild Dps (w-Dps) as well as CNHB-Dps. The dissociation constant measurements clearly indicated that the newly obtained Dps had higher adsorption capacity. Furthermore, it was shown that the N-terminus rather than the C-terminus was preferable for the modification of Dps subunits with peptide aptamers. It was also shown that the insertion of a short linker between the Dps subunit and peptide aptamers increased the adsorption ability.

2. Results and Discussion

2.1. Characterization of Carbon Surface

The carbon-coated QCM sensors were first observed with UHR FE-SEM. The gold surface morphology could be observed slightly through carbon layers, indicating that a carbon layer uniformly covered the gold surface (Figure S1). XPS analysis was conducted next (Figure 1). The wide-scan spectra showed two main signals of carbon C1s and oxygen O1s. The C1s signal was resolved into five components: sp^3 carbon with C-C bonds (283.8 eV), sp^2 carbon with C-C bonds (284.3 eV), C-O bonds (286 eV), C=O bonds (287 eV), and COO bonds (289 eV). The sp^2 carbon structure was about eight times more abundant than sp^3 at the top surface. The high oxygen content indicated that the surface was highly oxidized and presumed to be negatively charged.

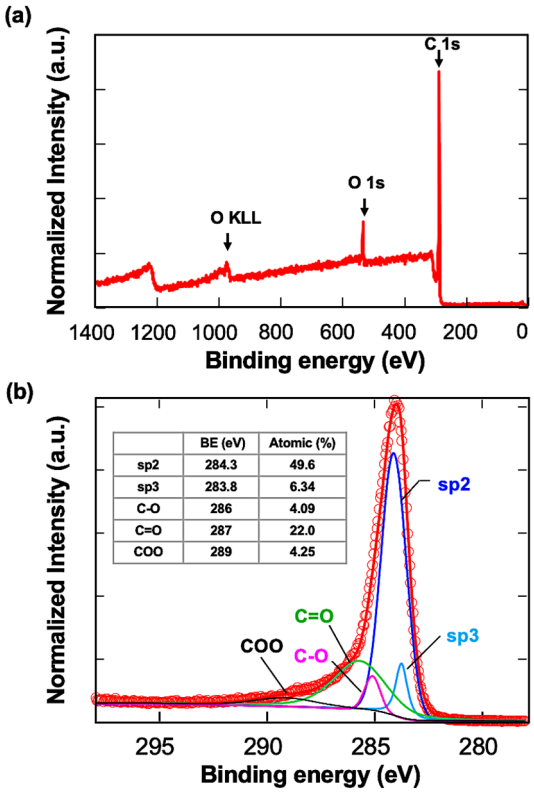

Figure 1. XPS analysis of the carbon-coated QCM sensors. (**a**) Wide spectrum of the sample, (**b**) spectrum of carbon components. The assignments are written in the table.

Raman measurement was also performed (Figure S2). The G and D bands were not separated and formed a broad peak. Since crystallinity affects the broadening of the peaks, it can be elucidated that the crystal structures of the deposited carbon layer were distorted and considered to have many defects. Peak separation results also showed a large D band peak and indicated a distorted structure and many defects.

2.2. QCM Measurements

2.2.1. Batch-Mode Measurements

The adsorption of Dps proteins onto a carbon-coated QCM sensor was measured at a 0.1 mg/mL concentration. Initially, a single measurement was performed for each protein, and the average values of ΔF1, ΔF2, and ΔF3 were used for the quantitative comparison of adsorption. The ΔF profiles of all proteins are shown in Figure 2. The differences between the initial baseline and the three resonance frequencies after repeated adsorption operations (DF_1, DF_2, DF_3) were recorded and averaged. The averaged ΔF and calculated Δm were 110.95 Hz and 39 ng/cm^2 for Y1Ct, 127.9 Hz and 46 ng/cm^2 for Y1Nt, 97.5 Hz and 35 ng/cm^2 for Y2Ct, 58.07 Hz and 21 ng/cm^2 for CNHB-Dps, and 24.17 Hz 8 ng/cm^2 for w-Dps. These results showed apparent quantitative differences. Y1Nt had the highest adsorption, followed by Y1Ct, Y2Ct, and CNBH-Dps. w-Dps had the lowest adsorption, which was nonspecific adsorption. However, as can be seen from the figure, the variation in ΔF was relatively large.

To minimize the influence of variation and allow for more precise quantitative discussion, the batch-mode experiment was repeated 10 times, and the average of 30 ΔF values was used to calculate the amount of adsorption for each protein (Table S1). The results are shown in Figure 3 and Table 1, where the vertical axis indicates the amount of protein adsorbed per cm^2, and the black bars indicate the standard deviation. The adsorption density of w-Dps was the lowest at 9.1 ng/cm^2, which could be determined as a normal nonspecific adsorption amount. On the other hand, Y1Nt showed 47.4 ng/cm^2, more than five times the nonspecific adsorption amount. Y1Ct also showed a high adsorption amount,

39.3 ng/cm^2. It was clearly indicated that the Y1 peptide achieved strong adsorption and addition to the N-terminus was more effective. In the case of Y2Ct, the adsorption amount was 35.4 ng/cm^2, which was four times higher than nonspecific adsorption and sufficiently high, but not as high as Y1Ct. Since the peptides were attached to the same C-terminus (Y1Ct, Y2Ct), the results should reflect the adsorption ability of Y1 and Y2. This result was consistent with the previous results that the Y2 peptide alone adsorbed less on the carbon surface than Y1. (Figure S4). The CNHB-Dps adsorbed 21.6 ng/cm^2, indicating that CNHB-Dps adsorbs specifically to the carbon surface, but not as much as the newly selected peptide aptamer.

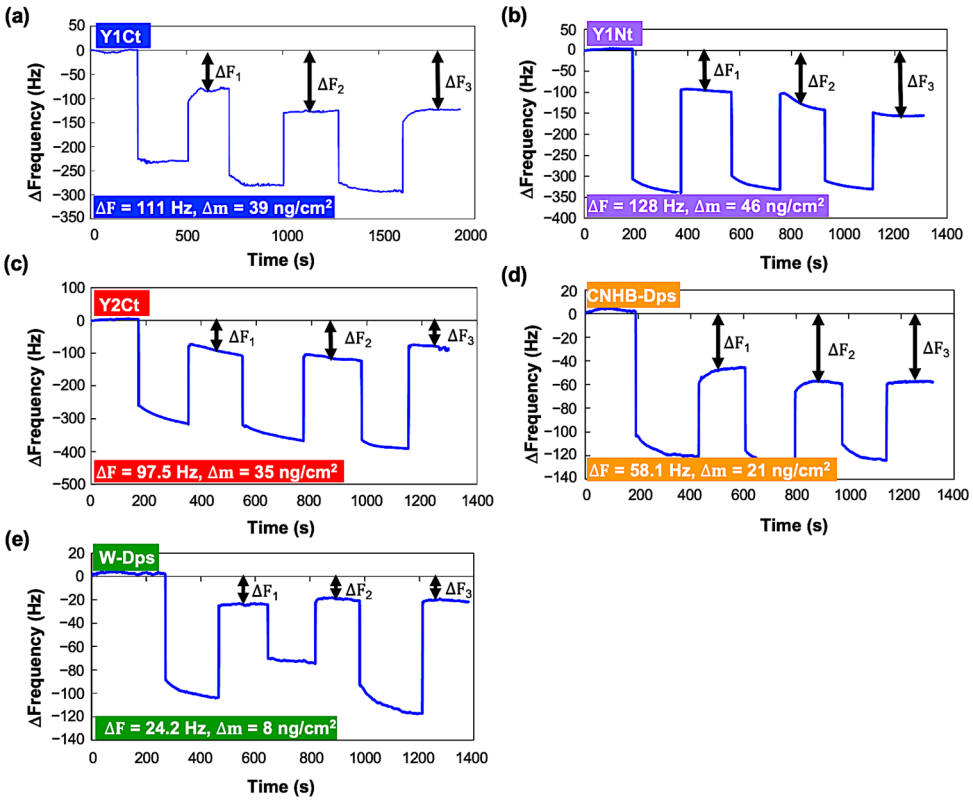

Figure 2. Changes in resonance frequency (ΔF) in the batch-mode measurements. The addition of each protein with a final concentration of 0.1 mg/mL and washing were repeated three times. (**a**) Y1Ct, (**b**) Y1Nt, (**c**) Y2Ct, (**d**) CNHB-Dps, and (**e**) w-Dps.

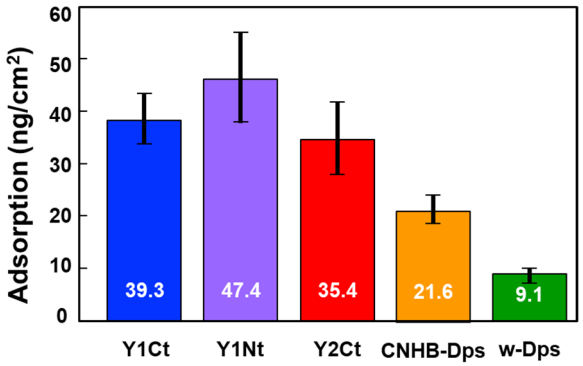

Figure 3. Average adsorption density values (mean ± S.D.) for Y1Ct, Y1Nt, Y2Ct, CNHB-Dps, and w-Dps onto the carbon surface. The values were calculated using the average of 30 DFs for each protein.

Table 1. Adsorption protein densities (Dm) and dissociation constants (Kd) obtained by the QCM batch- and flow-mode measurements.

	Y1Ct	Y1Nt	Y2Ct	Y1C	CNHB-Dps	w-Dps
(Batch-mode) Δm 30 Averaged	39.3 ng/cm^2	47.4 ng/cm^2	35.4 ng/cm^2	-	21.6 ng/cm^2	9.1 ng/cm^2
(Flow-mode) Kd	1.04 μM	0.74 μM	2.18 μM	3.02 μM	-	-

2.2.2. Open-Flow-Mode Measurement

Open-flow-mode measurements were performed using a closed chamber (QCM934-500, Seiko EG&G, Tokyo, Japan). After the system was stabilized, protein solutions with concentrations of 0.05 mg/mL, 0.1 mg/mL, 0.25 mg/mL, 0.5 mg/mL, 0.75 mg/mL, and 1 mg/mL were added at a flow rate of 50 μL/min. Resonance frequency change from the stabilized initial frequency, Δf, was recorded continuously. Figure 4 shows the results. Y1Ct, Y1Nt, Y2Ct, and Y1C exhibited similar trends. Δf showed small and slow changes at low concentrations and large and rapid decreases at high concentrations. The results were in agreement with the general adsorption behavior of proteins. However, the frequency change in CNHB-Dps was too small to be discernible, and w-Dps (without aptamer) did not yield a meaningful frequency change (Figure 4e,f). This indicates that w-Dps and CNHB-Dps had a low affinity to the carbon surfaces, which was already indicated by the batch-mode measurements. The dissociation constant, Kd, was determined using the commercial software (supplied with QCM934) (see Supporting Information and Figure S5). The results showed the good linearity of the determination coefficient (R^2). The Kd was 0.74 μM (R^2 = 0.99) for Y1Nt, 1.04 μM (R^2 = 0.95) for Y1Ct, 2.18 μM (R^2 = 0.98) for Y2Ct, and 3.02 μM (R^2 = 0.94) for Y1C (See Table 1). Y1Nt was the most strongly adsorbed with the lowest dissociation constant, followed by Y1Ct, Y2Ct, and Y1Ct. This result was consistent with batch-mode measurements, and the adsorption ability order was quantitatively proven. The Kd of CNHB-Dps and w-Dps could not be calculated.

We concluded that the adsorption ability of w-Dps and CNHB-Dps was quite small, while the newly selected aptamers, Y1 and Y2, gave Dps with high adsorption ability. The Dps with new peptides had much higher affinity than the previously available carbon nanohorn-binding peptides, as we had planned.

The Kd of Y1Nt (0.74 μM) was slightly smaller than Y1Ct (1.04 μM). The Y1 aptamer connected to the N-terminal of the Dps subunit worked more efficiently than that in the C-terminal position. The position and orientation of the aptamer might have contributed the difference. At the N-terminal, the peptide was bound in the same direction as when presented at M13 in the bio-panning process, but at the C-terminal in the opposite orientation. In N-terminal attachment, the N-terminus of the peptide was free to move and the C-terminus was fixed, whereas in C-terminal attachment, it was vice versa. This difference may account for the difference in adsorption capacity. The Kd was the smallest for Y1Nt. This is consistent with the QCM batch-mode results, in which Y1Nt showed the highest Δm value. Both Y1Nt (0.74 μM) and Y1Ct (1.04 μM) showed higher binding affinities than Y2Ct (2.18 μM), indicating that the Y1 aptamer was more efficient than the Y2 aptamer. This was also consistent with the batch-mode results and the adsorption ability of the peptide aptamers measured with electrochemical impedance spectroscopy (Figure S4). The lower affinity of Y1C (3.02 μM) compared with Y1Ct (1.04 μM) could be attributed to the absence of a linker. This result indicated that the linker was important for increasing absorbability. A flexible linker might help the aptamer move more freely, change direction, and interact more efficiently with the surface.

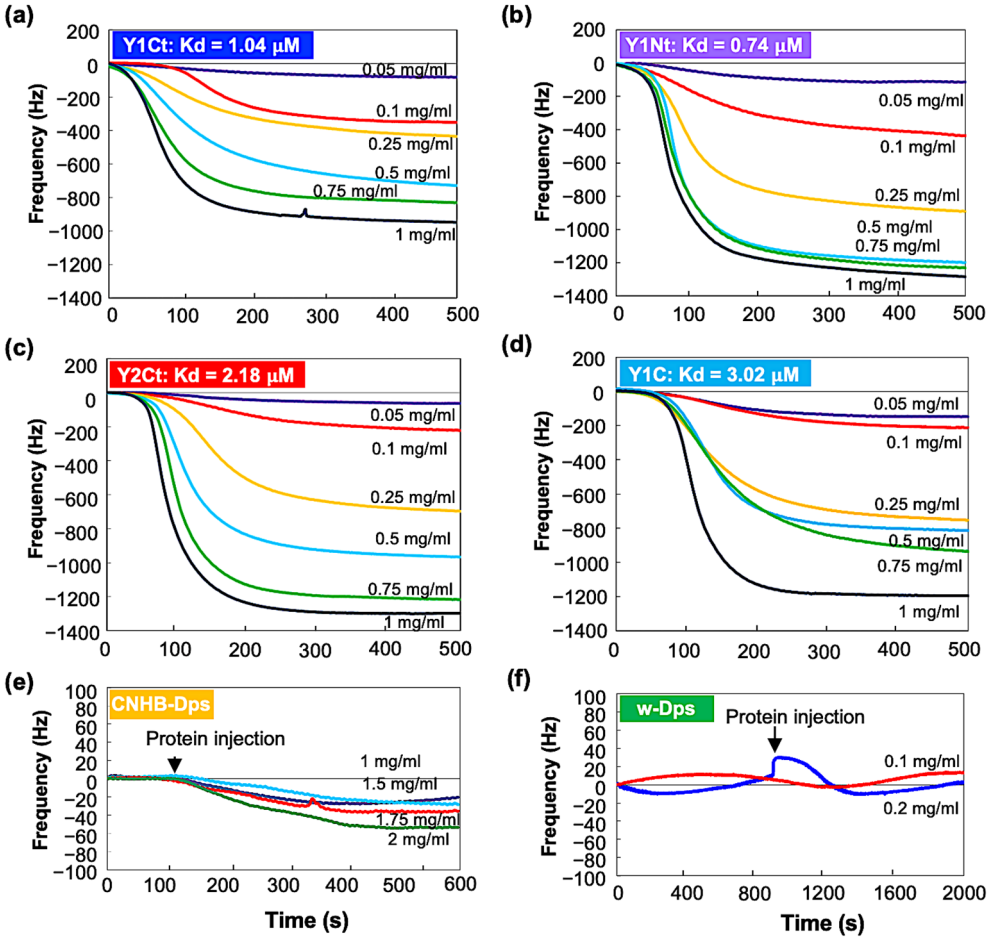

Figure 4. QCM open-flow measurement results of (**a**) Y1Ct, (**b**) Y1Nt, (**c**) Y2Ct, (**d**) Y1C, (**e**) CNHB-Dps, and (**f**) w-Dps on carbon-coated QCM sensor.

Although it was difficult to explain the adsorption mechanism by which Y1 and Y2 adsorb to carbon surfaces, one possible assumption was the following. The binding between aptamer-modified proteins and the carbon surface was considered to be mainly dictated by hydrophobic force, and electrostatic interactions assisted it. Carbon surfaces are known as hydrophobic and negatively charged from defects. It might be possible that the peptide's terminal hydrophobic amino acids first contacted the carbon surface by hydrophobic interactions, and at that time, the positively charged amino acid residues adjacent to the hydrophobic termini supported the adsorption efficiently. In the case of Y1Nt, hydrophobic phenylalanine (F) at the end and the next positively charged lysine (K) of the Y1 (FKQDAWEAVDIR) might play an important role in efficient binding. It was another possibility that phenylalanine engaged in aromatic stacking pi interactions with the carbon surface and played a role in influencing the initial interaction between Y1 and the carbon surface. In Y1Ct, the end was positively charged arginine (R) and the next was isoleucine (I); this difference in order might have made adsorption somewhat weaker. The lack of pi-tacking might also have something to do with it. In the Y2Ct case, Y2 (SYTHLLHRSLPG) had a hydrophobic end of glycine (G) and less hydrophilic proline (P) to the next. There was no positively charged amino acid near the terminal, which might have led to weaker adsorption.

3. Materials and Methods

3.1. Dps Protein Preparation

Wild Dps (w-Dps) and five types of mutant Dps were prepared for measurements (Figure 5). One of the mutants was Dps modified with carbon nanohorn binding peptide

(DYFSSPYYEQLF, CNHB-Dps). The rest were Dps modified with two kinds of CNT-binding peptide aptamers, Y1 (FKQDAWEAVDIR) and Y2 (SYTHLLHRSLPG), which we recently selected using the M13 phage display method [25]. Y1Nt; Y1 was genetically added to the N-terminus of the subunit via a linker (SGGG). Y1Ct; Y1 was added to the C-terminus of the subunit via a linker. Y1C; Y1 was added to the C-terminus of the subunit without a linker. Y2Ct; Y2 was added to the C-terminus of the subunit via a linker. Y1 and Y2 were predicted to adopt an alpha-helical conformation by 3D structural prediction (Figure S3) [25]. The dispersed charged amino acids ensured hydrophilicity, while adsorption to the carbon surface was thought to be based on hydrophobic interactions. The adsorption measurements of Y1 and Y2 on carbon screen-printed electrodes (SPEs) indicated that Y1 had affinity almost twice that of Y2 (Figure S4). Furthermore, it was shown that both Y1 and Y2 had higher adsorption abilities compared to the N- and C-terminal 12 amino acid sequence of Dps (DpsN, DpsC), which was considered to be a general hydrophilic peptide.

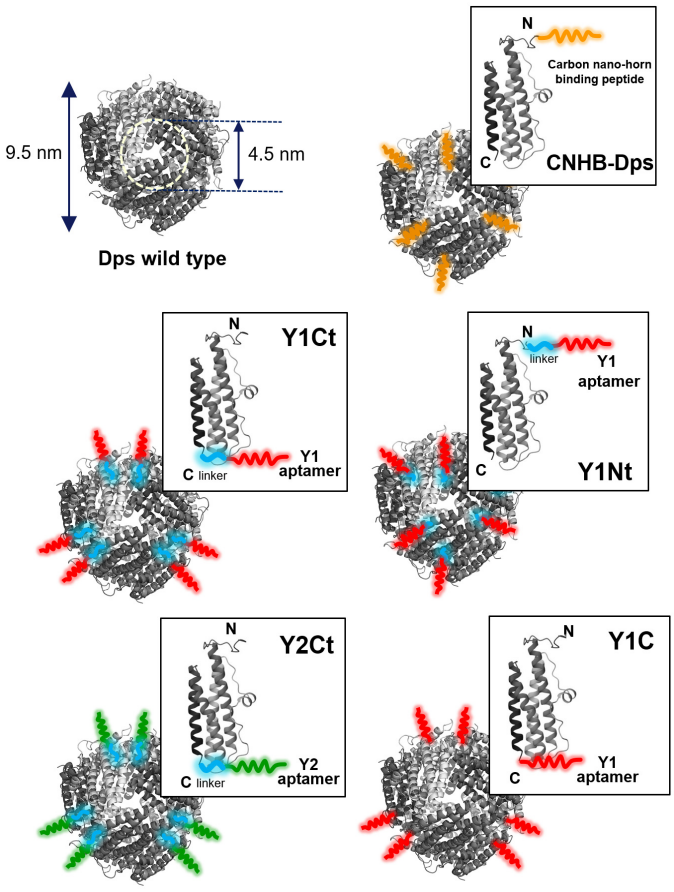

Figure 5. The cage-shaped protein Dps used in this work. Wild-type Dps (w-Dps, PDB) and mutant Dps with peptide aptamers. CNHB-Dps: carbon nanohorn-binding peptides were added at the N terminus of the Dps; Y1Ct and Y2Ct: Y1 and Y2 aptamers were genetically added at the C-terminus of the Dps with a linker; Y1Nt: Y1 aptamers were genetically added at the N-terminus of the Dps with a linker; Y1C: Y1 aptamers were genetically added at the C-terminus of the Dps without linker.

3.2. QCM Experiments

Applying alternating voltage to the AT-cut quartz crystal with a piezoelectric effect induces oscillations, generating a standing shear wave. When proteins were adsorbed, the resonant frequency decreased from its initial value, and the QCM can detect the mass of molecules adsorbed on the sensor with high accuracy, and kinetics can be calculated. The

QCM measurements of resonance frequency (Δf) decrease and energy dissipation (Δd) were performed using a QCM934 with a QA-CL4 well-type cell (Seiko EG&G, Tokyo, Japan). Commercially available gold QCM sensors (QA-A9M-AU(M)(SEP), Seiko EG&G, Tokyo, Japan) (Figure 6a) were coated with a carbon layer by vacuum evaporation and used for the experiments. The carbon surfaces were analyzed by an Ultra-High-Resolution Field Emission Scanning Electron Microscope (UHR FE-SEM, Hitachi SU9000, Tokyo, Japan), X-ray photoelectron spectroscopy (XPS, PHI 5000 Versa Probe II, ULVAC-PHI. Inc. Kanagawa, Japan) and Raman measurement (Laser Raman Spectrophotometer, NRS-4100-30, JASCO, Hachioji, Japan) (details are in the Supporting Information). Each sensor was used only once for each measurement. The sensor and chamber temperature was controlled at 25 ± 0.1 °C to ensure stable operation. Data were collected at 27 MHz (overtone number 3) and analyzed using the PS-P700/W32 WinQCMA software Ver.1.1.0.0 (Seiko EG&G). Two types of QCM measurements were performed, in batch and open-flow mode. In the batch modse (Figure 6b), a QCM sensor was first set in the measurement chamber, the chamber was filled with milli-Q water, and then, the resonance frequency recording was started. After the resonant frequency stabilized (the baseline resonance frequency), the cage-shaped protein was introduced into the chamber with a final concentration of 0.1 mg/mL. After the protein deposition on the sensor surface was confirmed by the decrease in resonance frequency, QCM measurement was halted, and the protein solution was removed. Milli-Q water was injected to wash away proteins weakly adsorbed on the sensor, and the resonance frequency was measured again (the resonance frequency after protein adsorption) to detect proteins adsorbed. The protein addition and washing were performed three times. The resonant frequency changes (ΔF1, ΔF2, and ΔF3, Figure 6b) were obtained by subtracting the average of the post-adsorption resonant frequency from the baseline resonant frequency. These three values were averaged to obtain the ΔF values for each measurement. The mass increase (Δm) by Dps molecules was calculated from these DF values using the Sauerbrey equation (Equation (1)). In this study, a 9 MHz AT-cut crystal with an electrode diameter of 5 mm and an overtone number of 3 had a sensitivity of −0.36 ng/Hz (about −1.8 ng/Hz/cm^2).

$$\Delta F = -\frac{2}{\sqrt{\mu\rho}} \times \frac{F^2}{n} \times \frac{\Delta m}{S} \quad (1)$$

where the terms are defined as follows:

ΔF: frequency change (Hz);
F: fundamental frequency;
Δm: mass change (g);
ρ: density of quartz (ρ = 2.648 g/cm^2);
S: piezoelectricity active crystal area (area between electrodes, cm^2);
μ: shear modulus of quartz for AT-cut crystal (μ = 2.947 × 1011 g/cm^2);
n: overtone number (n = 3 in this work).

In open-flow experiments (Figure 6c), the QCM sensor was set up in a flow chamber, and the QCM system was equilibrated with milli-Q water prior to measurements. The sensor was rinsed with milli-Q water at a constant flow rate of 50 µL/min using a peristaltic pump. This process stabilized the resonant frequency fluctuation to a level not exceeding 0.5 Hz for at least one hour, which ensured the stability and reliability of the experiment. After stabilization, a protein solution was introduced with a final concentration of 0.05 mg/mL to 1 mg/mL. The frequency change was continuously recorded until it was stabilized. The Kd of proteins on the carbon surface was kinetically evaluated from the open-flow experiment results.

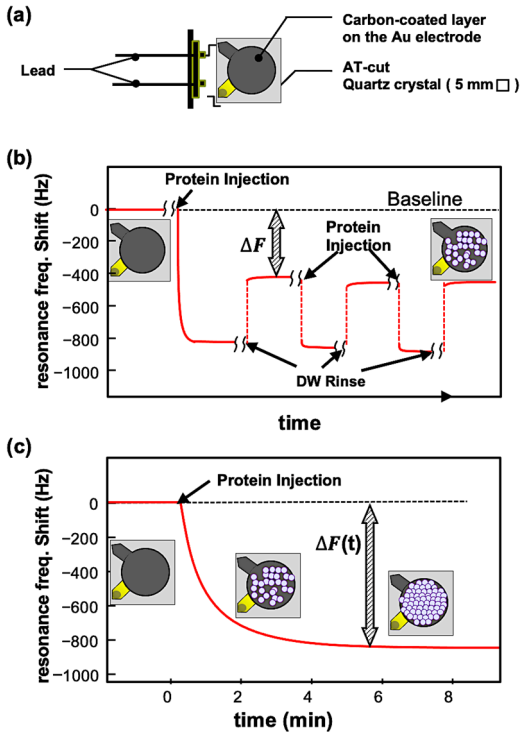

Figure 6. (**a**) Crystal sensor of QCM924. (**b**) Typical profile of frequency changes in the batch-mode measurement. The changes in frequency, DF, are defined as the difference between the baseline frequency and the frequency after the rinsing. (**c**) Typical profile of frequency changes in the open-flow measurement. In this measurement, the binding affinity of molecules on the surface can be kinetically evaluated using several measurements with different concentrations.

4. Conclusions

The adsorption behavior of cage-shaped proteins modified with newly selected peptide aptamers on carbon substrate was investigated using the QCM. The results successfully provided protein adsorption mass (Δm) and kinetic information (dissociation constant, Kd). In the batch-mode measurement, aptamer-modified proteins absorbed more than w-Dps (native Dps) and CNHB-Dps. In the open-flow-mode measurement, the dissociation constant, Kd, was obtained, which quantitatively showed that Y1Nt, Y1Ct, Y2Ct, and Y1C adsorbed more efficiently than w-Dps and CNHB-Dps onto the carbon surface. The results also proved that Y1 had higher affinity than the Y2 aptamer. Comparing Y1Nt and Y1Ct, the adsorption affinity of Y1Nt was higher, indicating that the aptamers attached to the N-terminal of the subunit enhanced the adsorption ability more effectively. It was also shown that the linker was important for improving protein adsorption. Even though the adsorption mechanism is hard to discuss, it could be assumed that the first hydrophobic end amino acid might initiate contact with the carbon surface, and nearby positively charged amino acids might help adsorption, achieving adsorption through hydrophobic interaction.

With the CNT-binding Dps fabricated in this study, CNT networks with a heterojunction, CNT/Dps (inner core)/CNT, would have higher thermoelectric performance. Furthermore, as shown in this study, the inorganic material-binding peptides selected by phage display were shown to retain their function even after being immobilized on the outer surface of the cage protein. In particular, it was shown that aptamer peptides maintained high binding capacity when attached to the N-terminus of the protein via a linker. Using the peptide-modified cage-shaped protein, the semiconducting nanoparticles synthesized inside the cage protein would be allowed to be placed only on the surface of the target material. In other words, semiconductor quantum dots can be placed on a specific surface fabricated by lithographic techniques, leading to quantum effect devices. If aptamers that interact with themselves were additionally immobilized, two-dimensional

crystals of Dps could be fabricated, and even more advanced functions could be achieved by the two-dimensional inner core using lateral electron tunneling. If nanoparticles of metals or oxides were encapsulated, the core could be used as the etching mask, and three-dimensional nanostructures and quantum structures could be created by etching layered bulk materials under the cores. Another easy nanostructure construction was achieved by Dps modified with electrode material-binding peptides and probe peptide aptamers. By simply dropping the solution droplets on the electrode and rinsing, electrodes for biosensing could be easily constructed. These are only some of the applications of aptamer-modified cage proteins, and the potential is enormous. We believe that this study will provide knowledge that will contribute to the construction of nanostructures using cage-shaped proteins.

Supplementary Materials: The following supporting information can be downloaded at https://www.mdpi.com/article/10.3390/biophysica4020018/s1, Figure S1: The SEM images of the Au (left) and carbon-coated (right) surfaces after deposition by the vacuum deposition. Figure S2: Raman spectra of carbon coated QCM sensors. Figure S3: Predicted 3D structures of Y1 and Y2 peptide aptamers and their characteristics of hydrophobicity and charge distribution. Figure S4: Rct increase with peptide aptamer adsorption. Each Rct was extracted from the EIS spectrum using a Randel equivalent circuit. The obtained Rct was normalized to the initial Rct (Rct0, no peptide). Figure S5: Kd determination from QCM results of (a) Y1Ct, (b) Y1t, (c) Y2Ct, and (d) Y1C. Approximate straight line obtained by the least squares method from the plot of each data is displayed in circle at different concentrations. Table S1. All DF and Dm obtained by the QCM batch-mode measurements.

Author Contributions: The manuscript was written with contributions from all authors. Conceptualization, analysis, N.G. and I.Y.; Methodology, N.G., T.-C.C., N.O. and K.I.; Writing—original draft, N.G.; Supervision, M.N. and I.Y. All authors have read and agreed to the published version of the manuscript.

Funding: This work is supported by Core Research for Evolutional Science and Technology, CREST (Grant No. JPMJCR18I3), from Japan Science and Technology Agency, JST.

Data Availability Statement: The data presented in this study are available on request from the corresponding author.

Acknowledgments: We thank HuanWen Han for the valuable comments and discussions on the structure, hydrophilicity, and electrostatic surface features of Y1 and Y2 peptides.

Conflicts of Interest: The authors declare no conflict of interest.

References

1. Ito, M.; Okamoto, N.; Abe, R.; Kojima, H.; Matsubara, R.; Yamashita, I.; Nakamura, M. Enhancement of thermoelectric properties of carbon nanotube composites by inserting biomolecules at nanotube junctions. *Appl. Phys. Express* **2014**, *7*, 065102. [CrossRef]
2. Roushani, M.; Rahmati, Z.; Hoseini, S.J.; Hashemi Fath, R. Impedimetric ultrasensitive detection of chloramphenicol based on aptamer MIP using a glassy carbon electrode modified by 3-ampy-RGO and silver nanoparticle. *Colloids Surf. B Biointerfaces* **2019**, *183*, 110451. [CrossRef] [PubMed]
3. Charbgoo, F.; Soltani, F.; Taghdisi, S.M.; Abnous, K.; Ramezani, M. Nanoparticles application in high sensitive aptasensor design. *TrAC Trends Anal. Chem.* **2016**, *85*, 85–97. [CrossRef]
4. Turner, A.P.F.; Karube, I.; Wilson, G.S. *Biosensors: Fundamentals and Applications*; Oxford University Press: Oxford, UK, 1987.
5. Barnes, L.M.; Lo, M.F.; Adams, M.R.; Chamberlain, A.H. Effect of Milk Proteins on Adhesion of Bacteria to Stainless Steel Surfaces. *Appl. Environ. Microbiol.* **1999**, *65*, 4543–4548. [CrossRef] [PubMed]
6. Yagati, A.K.; Choi, J.-W. Protein based electrochemical biosensors for H_2O_2 detection towards clinical diagnostics. *Electroanalysis* **2014**, *26*, 1259–1276. [CrossRef]
7. Nakanishi, K.; Sakiyama, T.; Imamura, K.J. On the adsorption of proteins on solid surfaces, a common but very complicated phenomenon. *Biosci. Bioeng.* **2001**, *91*, 233–244. [CrossRef]
8. Roach, P.; Farrar, D.; Perry, C.C. Interpretation of Protein Adsorption: Surface-Induced Conformational Changes. *J. Am. Chem. Soc.* **2005**, *127*, 8168–8173. [CrossRef]
9. Barnthip, N.; Parhi, P.; Golas, A.; Vogler, E.A. Volumetric interpretation of protein adsorption: Kinetics of protein-adsorption competition from binary solution. *Biomaterials* **2009**, *30*, 6495–6513. [CrossRef]
10. Uchida, M.; Klem, M.T.; Allen, M.; Suci, P.; Flenniken, M.; Gillitzer, E.; Varpness, Z.; Liepold, L.O.; Young, M.; Douglas, T. Biological Containers: Protein Cages as Multifunctional Nanoplatforms. *Adv. Mater.* **2007**, *19*, 1025–1042. [CrossRef]

11. Yamashita, I. Biological path for functional nanostructure fabrication and nanodevices. *Surf. Innov.* **2016**, *4*, 111–120. [CrossRef]
12. Okuda, M.; Suzumoto, Y.K.; Iwahori, K.; Kang, S.; Uchida, M.; Dougles, T.; Yamashita, I. Bio-templated CdSe nanoparticle synthesis in a cage shaped protein, Listeria-Dps, and their two dimensional ordered array self- assembly. *Chem. Commun.* **2010**, *46*, 8797–8799. [CrossRef] [PubMed]
13. Iwahori, K.; Enomoto, T.; Furusho, H.; Miura, A.; Nishio, K.; Mishima, Y.; Yamashita, I. CadmiumSulfide Nanoparticle Synthesis in Dps Protein from Listeria innocua. *Chem. Mater.* **2007**, *19*, 3105–3111. [CrossRef]
14. Iwahori, K.; Yamashita, I. Fabrication of CdS nanoparticles in the bio-template, apoferritin cavity by a slow chemical reaction system. *J. Phys. Conf. Ser.* **2007**, *61*, 492–496. [CrossRef]
15. Higo, A.; Kiba, T.; Chen, S.; Chen, Y.; Tanikawa, T.; Thomas, C.; Lee, C.Y.; Lai, Y.-C.; Ozaki, T.; Takayama, J.; et al. Optical Study of Sub-10 nm $In_{0.3}Ga_{0.7}N$ Quantum Nanodisks in GaN Nanopillars. *ACS Photon.* **2017**, *4*, 1851–1857. [CrossRef]
16. Huang, C.-H.; Wang, X.-Y.; Igarashi, M.; Murayama, A.; Okada, Y.; Yamashita, I.; Samukawa, S. Optical absorption characteristic of highly ordered and dense two-dimensional array of silicon nanodiscs. *Nanotechnology* **2011**, *22*, 105301. [CrossRef] [PubMed]
17. Budiman, M.F.; Hu, W.; Igarashi, M.; Tsukamoto, R.; Isoda, T.; Itoh, K.M.; Yamashita, I.; Murayama, A.; Okada, Y.; Samukawa, S. Control of optical bandgap energy and optical absorption coefficient by geometric parameters in sub-10 nm silicon-nanodisc array structure. *Nanotechnology* **2012**, *23*, 065302. [CrossRef]
18. Kobayashi, M.; Tomita, S.; Sawada, K.; Shiba, K.; Yanagi, H.; Yamashita, I.; Uraoka, Y. Chiral meta- molecules consisting of gold nanoparticles and genetically engineered tobacco mosaic virus. *Opt. Express* **2012**, *20*, 24856–24863. [CrossRef] [PubMed]
19. Cho, Y.; Okamoto, N.; Yamamoto, S.; Obokata, S.; Nishioka, K.; Benten, H.; Nakamura, M. Carbon Nanotube/Biomolecule Composite Yarn for Wearable Thermoelectric Applications. *ACS Appl. Energy Mater.* **2022**, *5*, 3698–3705. [CrossRef]
20. Brown, S. Metal-recognition by repeating polypeptides. *Nat. Biotechnol.* **1997**, *15*, 269–272. [CrossRef] [PubMed]
21. Sarikaya, M.; Tamerler, C.; Jen, A.K.; Schulten, K.; Baneyx, F. Molecular biomimetics: Nanotechnology through biology. *Nat. Mater.* **2003**, *2*, 577–585. [CrossRef]
22. Sano, K.; Shiba, K. A Hexapeptide Motif that Electrostatically Binds to the Surface of Titanium. *J. Am. Chem. Soc.* **2003**, *125*, 14234–14235. [CrossRef] [PubMed]
23. Okamoto, N.; Iwahori, K.; Yamashita, I. Silicon-Dioxide-Specific Peptides for Biological Nanofabrication. *IEEE Nanotechnol. Mag.* **2019**, *6*, 43–48. [CrossRef]
24. Kase, D.; Kulp, J.L.I.; Yudasaka, M.; Evans, J.S.; Iijima, S.; Shiba, K. Affinity selection of peptide phage libraries against single-wall carbon nanohorns identifies a peptide aptamer with conformational variability. *Langmuir* **2004**, *20*, 8939–8941. [CrossRef] [PubMed]
25. Han, H.-W.; Chu, T.-C.; Okamoto, N.; Nakamura, M.; Yamashita, I. CNT binding peptides selected by the phage display method. *Langmuir* **2023**, *39*, 14204. [CrossRef] [PubMed]
26. Grant, R.A.; Fliman, D.J.; Finkel, S.E.; Kolter, R.; Hoglem, J.M. The crystal structure of Dps a ferritin homolog that binds and protects DNA. *Nat. Struct. Biol.* **1998**, *4*, 294–303. [CrossRef] [PubMed]
27. Somorjai, G.A.; York, R.L.; Butcher, D.; Park, J.Y. The evolution of model catalytic systems; studies of structure, bonding and dynamics from single crystal metal surfaces to nanoparticles, and from low pressure (10−3 Torr) to liquid interfaces. *Phys. Chem. Chem. Phys.* **2007**, *9*, 3500–3513. [CrossRef]
28. Mermut, O.; Phillips, D.C.; York, R.L.; McCrea, K.R.; Ward, R.S.; Somorjai, G.A. In situ adsorption studies of a 14-amino acid leucine-lysine peptide onto hydrophobic polystyrene and hydrophilic silica surfaces using quartz crystal microbalance, atomic force microscopy, and sum frequency generation vibrational spectroscopy. *J. Am. Chem. Soc.* **2006**, *128*, 3598–3607. [CrossRef]